

# BRIGHT: A Collaborative Generalist-Specialist Foundation Model for Breast Pathology

Xiaojing Guo<sup>1,†,\*</sup>, Jiatai Lin<sup>2,3,†</sup>, Yumian Jia<sup>1,†</sup>, Jingqi Huang<sup>5,†</sup>, Zeyan Xu<sup>4,†</sup>, Weidong Li<sup>1,†</sup>, Longfei Wang<sup>5</sup>, Jingjing Chen<sup>6</sup>, Qin Li<sup>7</sup>, Weiwei Wang<sup>8</sup>, Lifang Cui<sup>9</sup>, Wen Yue<sup>10</sup>, Zhiqiang Cheng<sup>11</sup>, Xiaolong Wei<sup>12</sup>, Jianzhong Yu<sup>13</sup>, Xia Jin<sup>14</sup>, Baizhou Li<sup>15,16</sup>, Honghong Shen<sup>17</sup>, Jing Li<sup>18</sup>, Chunlan Li<sup>19</sup>, Yanfen Cui<sup>20</sup>, Yi Dai<sup>21</sup>, Yiling Yang<sup>1</sup>, Xiaolong Qian<sup>1</sup>, Liu Yang<sup>1</sup>, Yang Yang<sup>1</sup>, Guangshen Gao<sup>1</sup>, Yaqing Li<sup>1</sup>, Lili Zhai<sup>1</sup>, Chenying Liu<sup>1</sup>, Tianhua Zhang<sup>1</sup>, Zhenwei Shi<sup>2,3</sup>, Cheng Lu<sup>2,3</sup>, Xingchen Zhou<sup>22</sup>, Jing Xu<sup>23</sup>, Miaoqing Zhao<sup>24,\*</sup>, Fang Mei<sup>25,\*</sup>, Jiaojiao Zhou<sup>26,27,\*</sup>, Ning Mao<sup>28,29,30,31,\*</sup>, Fangfang Liu<sup>1,\*</sup>, Chu Han<sup>2,3,4,\*</sup>, and Zaiyi Liu<sup>2,3,4,\*</sup>

<sup>1</sup>Department of Breast Pathology and Laboratory, Tianjin Medical University Cancer Institute & Hospital, National Clinical Research Center for Cancer, Key Laboratory of Breast Cancer Prevention and Therapy, Tianjin Medical University, Ministry of Education, Tianjin's Clinical Research Center for Cancer, West Huanhu Road, Tianjin, China

<sup>2</sup>Guangdong Provincial Key Laboratory of Artificial Intelligence in Medical Image Analysis and Application, Guangdong Provincial People's Hospital (Guangdong Academy of Medical Sciences), Southern Medical University, Guangzhou, China

<sup>3</sup>Department of Radiology, Guangdong Provincial People's Hospital (Guangdong Academy of Medical Sciences), Southern Medical University, Guangzhou, China

<sup>4</sup>Department of Radiology, Yunnan Cancer Hospital, The Third Affiliated Hospital of Kunming Medical University, Peking University Cancer Hospital Yunnan, Yunnan, China

<sup>5</sup>School of Biomedical Engineering, Southern Medical University, Guangzhou, China

<sup>6</sup>Department of Radiology, Qingdao University Hospital, Qingdao, Shandong, China

<sup>7</sup>Department of Medical Imaging, Weifang Hospital of Traditional Chinese Medicine, Weifang, Shandong, China

<sup>8</sup>Department of Medical Imaging, Affiliated Hospital of Jining Medical University, Jining, Shandong, China

<sup>9</sup>Department of Pathology, China-Japan Friendship Hospital, Beijing, China

<sup>10</sup>Department of Pathology, The Obstetrics & Gynecology Hospital of FuDan University, Shanghai, China

<sup>11</sup>Department of Pathology, ShenZhen Third People's Hospital, Guangdong, China

<sup>12</sup>Department of Pathology, Cancer Hospital of ShanTou University Medical College, Guangdong, China

<sup>13</sup>Department of Pathology, DongGuan People's Hospital, Guangdong, China

<sup>14</sup>Department of Pathology, Hunan Cancer Hospital, The Affiliated Cancer Hospital of Xiangya School of Medicine, Central South University, Hunan, China

<sup>15</sup>Department of Pathology, The Second Affiliated Hospital Zhejiang University School of Medicine, Zhejiang, China

<sup>16</sup>Department of Pathology, The Fourth Affiliated Hospital, Zhejiang University School of Medicine, Zhejiang, China

<sup>17</sup>Department of Pathology, Second hospital of ShanXi Medical University, ShanXi, China

<sup>18</sup>Department of Pathology, ZiBo Central Hospital, Shandong, China

<sup>19</sup>Department of Pathology, QiLu Hospital of Shandong University, Shandong, China

<sup>20</sup>Department of Radiology, Shanxi Province Cancer Hospital, Shanxi Hospital Affiliated to Cancer Hospital, Chinese Academy of Medical Sciences/Cancer Hospital Affiliated to Shanxi Medical University, Shanxi, China

<sup>21</sup>Department of Medical Imaging, Peking University Shenzhen Hospital, Guangdong, China

<sup>22</sup>Department of Pathology, The Second Hospital, Cheeloo College of Medicine, Shandong University

<sup>23</sup>Department of Pathology, Qingdao Central Hospital, University of Health and Rehabilitation Sciences, Qingdao, China

<sup>24</sup>Department of Pathology, Shandong First Medical University Affiliated Tumor Hospital, Shandong, China

<sup>25</sup>Department of Pathology, Peking University Third Hospital, School of Basic Medical Sciences, Peking University Health Science Center, Beijing, China

<sup>26</sup>Department of Breast Surgery and Oncology, the Second Affiliated Hospital, Zhejiang University School of Medicine, Hangzhou, China

<sup>27</sup>The Key Laboratory of Cancer Prevention and Intervention, China

<sup>28</sup>Big Data and Artificial Intelligence Laboratory, Yantai Yuhuangding Hospital, Qingdao University, Yantai, Shandong, China

<sup>29</sup>Department of Radiology, Yantai Yuhuangding Hospital, Qingdao University, Yantai, Shandong, China

<sup>30</sup>Shandong Provincial Key Medical and Health Laboratory of Intelligent Diagnosis and Treatment for Women's Diseases, Yantai Yuhuangding Hospital, Qingdao University, Yantai, Shandong, China

<sup>31</sup>Faculty of Applied Sciences, Macao Polytechnic University, Macao, China

†These authors contributed equally to this work.

\*Correspondence: guoxiaojing@tjmuch.com (Xiaojing Guo), zhaomqsd@163.com (Miaoqing Zhao), meifangmail@bjmu.edu.cn (Fang Mei), zhoujj@zju.edu.cn (Jiaojiao Zhou), maoning@pku.edu.cn (Ning Mao), liufangfang@tjmuch.com (Fangfang Liu), hanchu@gdph.org.cn (Chu Han), liuzaiyi@gdph.org.cn (Zaiyi Liu)

## ABSTRACT

Generalist pathology foundation models (PFMs), pretrained on large-scale multi-organ datasets, have demonstrated remarkable predictive capabilities across diverse clinical applications. However, their proficiency on the full spectrum of clinically essential tasks within a specific organ system remains an open question due to the lack of large-scale validation cohorts for a single organ as well as the absence of a tailored training paradigm that can effectively translate broad histomorphological knowledge into the organ-specific expertise required for specialist-level interpretation. In this study, we propose BRIGHT, the first PFM specifically designed for breast pathology, trained on approximately 210 million histopathology tiles from over 51,000 breast whole-slide images derived from a cohort of over 40,000 patients across 19 hospitals. BRIGHT employs a collaborative generalist-specialist framework to capture both universal and organ-specific features. To comprehensively evaluate the performance of PFMs on breast oncology, we curate the largest multi-institutional cohorts to date for downstream task development and evaluation, comprising over 25,000 WSIs across 10 hospitals. The validation cohorts cover the full spectrum of breast pathology across 24 distinct clinical tasks spanning diagnosis, biomarker prediction, treatment response and survival prediction. Extensive experiments demonstrate that BRIGHT outperforms three leading generalist PFMs, achieving state-of-the-art (SOTA) performance in 21 of 24 internal validation tasks and in 5 of 10 external validation tasks with excellent heatmap interpretability. By evaluating on large-scale validation cohorts, this study not only demonstrates BRIGHT's clinical utility in breast oncology but also validates a collaborative generalist-specialist paradigm, providing a scalable template for developing PFMs on a specific organ system, accelerating the translation of foundation models into specialized clinical practice.

## KEYWORDS

Computational pathology, Foundation model, Breast cancer, Generalist-specialist collaboration

## Introduction

The advent of computational pathology (CPath)<sup>1</sup>, powered by deep learning<sup>2</sup>, holds transformative potential for oncology. By extracting sub-visual features from whole-slide images (WSIs), CPath techniques promise to augment pathological diagnosis<sup>3,4</sup>, predict molecular profiles<sup>5-7</sup>, treatment response<sup>8</sup> and patient prognosis<sup>9-11</sup>, thereby advancing the goals of precision medicine. However, the clinical translation of these models has been largely constrained by a dominant paradigm of developing narrow, task-specific models. They are typically trained on limited, single-institution datasets for a singular clinical endpoint, resulting in unsatisfactory performance and poor generalization across diverse clinical settings.

Given the pressing need of scalable AI in pathology, a new paradigm of Pathology Foundation Models (PFMs) has emerged. Inspired by breakthroughs in computer vision, recent studies have adapted state-of-the-art self-supervised learning (SSL) algorithms<sup>12,13</sup> to train models on vast and diverse multi-organ WSI datasets<sup>14-24</sup>. This pre-training strategy allows a model to learn a universal and transferable representation of fundamental histopathological patterns without any manual annotation<sup>25</sup>. Once established, such a generalist PFM can be efficiently adapted with minimal labeled data to a wide array of downstream clinical tasks. Furthermore, the benefits also include robust performance in data-limited (few-shot) settings, zero-shot capabilities, and significantly faster convergence during task-specific training compared to models trained from scratch<sup>21</sup>.

Despite their demonstrated versatility, the capability and generalizability of existing generalist PFMs when applied to the comprehensive clinical workflow of a single, specialized organ system remain unclear for the following two reasons. From the benchmarking perspective, the field of CPath is actually constrained by a severe scarcity of large-scale, open-source pathology datasets<sup>26</sup>. Compounded by the inherent difficulty of assembling sufficient private data for a specific organ, most generalist PFM studies evaluated their organ-specific performance on limited public datasets. Consequently, these evaluations rely on data that are typically small in scale, lack the heterogeneity of real-world clinical practice and finally fail to encompass the full spectrum of diagnostic, prognostic and predictive tasks required for comprehensive organ-specific assessment. Even dedicated PFM benchmarking studies currently lack the necessary organ-focused, task-comprehensive cohorts<sup>27-29</sup>. Such a design measures

multi-organ versatility rather than depth of expertise within a single domain, leaving a critical gap from generalist to specialist. From the technical perspective, current generalist PFMs are primarily developed using multi-organ datasets. While this strategy effectively learns universal histomorphological patterns, it might fail to represent the organ-specific expertise features that are critical for specialist-level interpretation within a single organ system. This limitation is further corroborated by evidence suggesting that different PFMs, pretrained with distinct strategies on varied datasets, exhibit specialized advantages on different evaluation tasks<sup>24</sup>.

In this study, we introduce BRIGHT (**BR**east **patHoloGy** **foundaTI**on model), a collaborative generalist-specialist framework designed to establish the first PFM for breast pathology. Since existing PFMs have already learned the generalist histomorphological patterns very well. The core idea of BRIGHT is to integrate the well-learned generalist features with the specialist organ-specific features learned from breast pathology data. We first train a specialist model BRIGHT (S) from a leading PFM Virchow2<sup>22,30</sup> that trained on over 3 million WSIs, using an efficient and parameter-effective fine-tuning strategy low-rank adaptation (LoRA)<sup>31</sup> to adapt the generalist foundation to the specialized domain of breast pathology (Figure 1c). Then we integrate the feature representations by collaboratively fusing the generalist feature embeddings extracted from the original Virchow2 encoder with the specialist feature embeddings extracted from the adapted BRIGHT (S) encoder. This collaborative generalist-specialist architecture enables BRIGHT to simultaneously leverage broad histomorphological understanding and nuanced, breast-specific diagnostic insights.

BRIGHT is pre-trained on approximately 210 million histopathology tiles extracted from 51,836 breast WSIs (Figure 1c), including 42,876 WSIs sourced from a five-year, consecutively collected data of 32,054 patients from our primary cohort (C1.TMUCIH) and 8,960 WSIs across 18 major institutions. As a result, both training and validation cohorts comprehensively cover various breast disease types, spanning almost the entire spectrum from benign lesions, in situ carcinomas, to invasive carcinomas of various histological and molecular subtypes. It ensures that BRIGHT learns a rich and diverse feature representation of breast-specific pathology and provides a robust basis for evaluating the real-world clinical performance of PFMs. To thoroughly evaluate BRIGHT and the broader capabilities of PFMs in breast oncology, we have established a comprehensive benchmarking dataset comprising 24 clinically essential tasks. These tasks span the full clinical workflow, including diagnosis, biomarker prediction, treatment response assessment, and survival prediction (Figure 1a). The development and validation of the downstream models are supported by the cohort with over 25,000 of WSIs which is much larger than existing PFM benchmarking studies (Figure 1b). This substantial scale ensures more robust and stable model training than that trained on limited samples, providing a reliable reflection of real-world clinical performance. Furthermore, the size and diversity of these cohorts enable meaningful subgroup modeling to evaluate predictive performance across different treatment strategies for different molecular subtypes.

We comprehensively evaluate BRIGHT across 24 benchmarks (Figure 1d) covering the full spectrum of the clinical applications. BRIGHT generally outperforms existing generalist PFMs and the specialist model BRIGHT (S), reflecting the efficacy of the collaborative generalist-specialist design. Notably, BRIGHT achieves top-1 (top-2) performance in 21 (24) out of 24 internal tasks (Figure 1e) and 5 (8) out of 10 external tasks (Figure 1f). These findings highlight BRIGHT not only as a state-of-the-art model for breast oncology but also as a scalable template for developing high-fidelity, organ-specific foundation models, thereby accelerating the translation of artificial intelligence into specialized clinical practice.

## Results

The BRIGHT model was pre-trained on a large-scale, diverse cohort of breast WSIs, encompassing the full pathological spectrum from benign lesions and in situ carcinomas to invasive carcinomas of varied histological and molecular subtypes. This comprehensive training enables BRIGHT to learn a rich and diverse feature representation of breast-specific pathology. To rigorously assess its clinical utility, we evaluated BRIGHT-derived feature embeddings across 24 distinct downstream tasks, spanning four major clinical domains, including histological diagnosis, biomarker prediction, treatment response prediction and prognosis prediction. Following the established weakly-supervised paradigm in computational pathology, we employed a multiple-instance learning (MIL) framework CLAM<sup>32</sup> for task-specific downstream adaptation. For a robust internal evaluation, we constructed a held-out validation cohort comprising all consecutive patients undergoing breast biopsy from the full calendar year of 2024 at our primary institution (C1.TMUCIH), ensuring a natural and unselected distribution reflective of real-world breast oncology practice. To evaluate the generalizability of BRIGHT, external validation is conducted on the WSIs collected from 9 external hospitals. To ensure a rigorous and unbiased evaluation, all WSIs used for downstream task assessment were held-out from the BRIGHT foundation model's pre-training phase. The detailed dataset distribution of each task is shown in Supplementary Table S1 (primary cohort) and S2 (external cohorts). We compare BRIGHT with three leading PFMs, including two image-based PFMs (Virchow2<sup>22,30</sup> and UNIV<sup>21</sup>), one visual-language PFM (CONCHv1.5<sup>17</sup>) as well as the specialist version of BRIGHT (S).

## **BRIGHT can enhance diagnostic accuracy**

We first evaluate the diagnostic performance of BRIGHT on, to our knowledge, the most comprehensive and largest curated dataset for breast pathology, comprising a total of 18,250 WSIs for downstream task development, 4,107 WSIs for internal validation and 1,559 WSIs from 4 independent hospitals for external validation (Figure 2a). The diagnostic benchmark encompasses six clinically essential tasks, including breast cancer detection, multi-class histological subtyping, Nottingham histologic grading, tumor-infiltrating lymphocytes (TILs) assessment, lymph node metastasis prediction (N-stage), and pathological TNM (pTNM) staging. To further assess generalizability, we also evaluate performance on the publicly available BRACS dataset<sup>33</sup>.

BRIGHT demonstrates state-of-the-art (SOTA) diagnostic performance, generally outperforming all benchmarked PFMs across every diagnostic task on the internal validation set (Figure 2b). For breast cancer detection, BRIGHT achieves an exceptional AUC of 0.992 (95%CI: 0.989-0.994) on the natural-distribution cohort (Figure 2c), confirming its robustness and potential as a clinically viable tool to support primary screening and reduce pathologist workload with high reliability. For the more challenging multi-class histological diagnosis task, BRIGHT outperforms SOTA PFMs. It achieves an AUC of 0.973 (95%CI: 0.965-0.980), a weighted F1-score of 0.901 and a top-1 accuracy of 0.899 (95%CI: 0.889-0.909) (Figure 2e-f). Notably, BRIGHT shows outstanding classification performance for high-prevalence categories (Figure 2d) such as invasive carcinoma (IC), ductal carcinoma in situ (DCIS) and papillary neoplasms (PN), while providing accurate and interpretable attention heatmaps that align with pathological diagnostic criteria (Figure 2h). The combination of high accuracy and explainability is critical for reliable triage and diagnostic support in routine clinical practice. Across the remaining diagnostic spectrum, BRIGHT achieves AUCs of 0.898 (95%CI: 0.885-0.912) for Nottingham histologic grading, 0.967 (95%CI: 0.950-0.982) for TILs assessment, 0.968 (95%CI: 0.951-0.982) for lymph node metastasis prediction and 0.661 (95%CI: 0.641-0.682) for pTNM staging. BRIGHT also outperforms other PFMs on the 7-class histological diagnosis on BRACS with only 547 WSIs (394 WSIs for model training), which demonstrates the capability on limited training samples (Figure 2b). The model's performance is further validated on two independent external cohorts, confirming its generalizability across diverse clinical and institutional settings (Figure 2g). Comprehensive performance metrics for each model and diagnostic tasks are provided in Supplementary Table S6-S8.

## **BRIGHT advances molecular subtyping and biomarkers prediction**

Beyond histomorphological diagnosis, the prediction of molecular biomarkers and subtypes from routine H&E slides represents a transformative application of computational pathology. We rigorously evaluated BRIGHT alongside benchmark PFMs on a comprehensive panel of seven immunohistochemistry (IHC) biomarkers, including estrogen receptor (ER), progesterone receptor (PR), human epidermal growth factor receptor 2 (HER2), Ki-67, androgen receptor (AR), cytokeratin 5/6 (CK5/6), and epidermal growth factor receptor (EGFR). Reflecting recent therapeutic advances, our evaluation includes a clinically critical three-tier HER2 classification task (HER2-zero, HER2-low, and HER2-positive), motivated by evidence that trastuzumab deruxtecan (T-DXd) improves overall and progression-free survival in HER2-low patients compared to standard chemotherapy<sup>34,35</sup>. Furthermore, given the growing importance of immunotherapy, we also evaluate the prediction of programmed death-ligand 1 (PD-L1) expression, a key biomarker for immune checkpoint inhibitor response<sup>36</sup>. Finally, we assess the model's ability on the prediction of the four major molecular subtypes (Luminal A, Luminal B, HER2-enriched, and Triple-negative breast cancer).

On the large-scale internal validation set (Figure 3a), BRIGHT achieved the highest AUROC in most of the biomarker prediction tasks, attaining an average AUC of 0.938 (95%CI: 0.926-0.948) for ER, 0.912 (95%CI: 0.897-0.925) for PR, 0.902 (95%CI: 0.888-0.918) for Ki-67, 0.877 (95%CI: 0.858-0.894) for HER2 (binary classification), 0.796 (95%CI: 0.779-0.812) for HER2 (three-tier classification), 0.952 (95%CI: 0.933-0.968) for AR, 0.918 (95%CI: 0.900-0.934) for CK5/6, and 0.864 (95%CI: 0.843-0.883) for EGFR (Figure 3b). Furthermore, BRIGHT demonstrated superior performance in predicting the integrated molecular subtype compared to all benchmarked PFMs with AUC of 0.875 (95%CI: 0.862-0.887). Notably, even for the challenging task of PD-L1 prediction with only 289 training samples, BRIGHT achieves a higher AUC of 0.938 (95%CI: 0.814-1.000). This result underscores the model's data-efficient nature, which is a critical attribute for translating biomarker prediction tools to clinical settings where large-scale cohorts may not always be available. Comprehensive performance metrics for each model and related tasks on internal test set are provided in Supplementary Table S9.

Additionally, based on the integrated molecular subtype prediction task and its required four key biomarkers (ER, PR, HER2, Ki-67), we conduct an independent external validation experiment to rigorously assess the model's generalizability. This combined external cohort comprises data from 6 independent medical centers and includes the publicly available TCGA-BRCA dataset, ensuring diverse clinical settings. BRIGHT demonstrates outstanding model generalizability with highly stable classification performance comparing with the baseline models (Figure 3c), demonstrating its robustness across diverse and real-world clinical settings. Interpretability analysis reveals that BRIGHT's attention maps show high visual concordance (Figure 3e) with the expression of corresponding IHC across four key biomarkers for each molecular subtype, greatly improving the trustworthiness of BRIGHT's prediction. Comprehensive performance metrics for each model and related tasks on external

test set are provided in Supplementary Table S10.

To directly quantify the potential clinical utility of BRIGHT for biomarker prediction, we estimated its capacity to reduce the need for IHC assays. By applying dual clinical thresholds (high Negative Predictive Value, NPV, and high Positive Predictive Value, PPV) to BRIGHT's prediction scores, we identify a substantial subset of cases where IHC testing could be potentially waived with high confidence (Figure 3d). For instance, at a conservative NPV/PPV threshold of 0.98, BRIGHT could reduce the need for IHC testing by approximately 61.4% for ER, 32.1% for PR, 30.9% for Ki-67, 19.0% for HER2, 91.7% for AR, 13.0% for CK5/6, 9.1% for EGFR and 47.2% for PD-L1. Even under the most stringent threshold of 1.0, BRIGHT still achieves a notable reduction of approximately 2.3%-47.2% across these biomarkers. It brings a substantial acceleration of the conventional diagnostic pathway, reducing the time for biomarker confirmation from several days to just minutes, demonstrating BRIGHT's concrete potential to accelerate diagnostic workflows and reduce associated costs without compromising diagnostic accuracy.

### **BRIGHT can predict therapeutic response**

Neoadjuvant therapy (NAT) represents a cornerstone of breast cancer management, aiming to downstage tumors prior to surgery and potentially obviate the need for extensive resection for the cases of pathological complete response (pCR). However, predicting patient response to NAT from pre-treatment histology represents a major yet unmet goal in precision oncology for breast cancer. We evaluated the efficacy of BRIGHT on predicting NAT outcomes using diagnostic H&E biopsy slides obtained prior to treatment.

On the held-out internal validation cohort, BRIGHT achieves superior performance in predicting pCR to neoadjuvant therapy (AUC: 0.786 (95%CI: 0.753-0.817)) compared to all benchmarking PFMs (Figure 4b). This predictive advantage is generally maintained on the independent multi-center external validation set (AUC: 0.641 (95%CI: 0.609-0.667)), Figure 4c), demonstrating robust generalizability. Since neoadjuvant therapeutic strategies for breast cancer are highly subtype-specific. For example, HER2-positive breast cancer requires a dual-blockade strategy combining trastuzumab and pertuzumab with chemotherapy<sup>37</sup>, whereas the standard of care for high-risk triple-negative breast cancer (TNBC) has shifted towards platinum-containing chemotherapy combined with immune checkpoint inhibitors<sup>38</sup>. Thus, we leveraged our large-scale cohort (Figure 4a) to perform subgroup-specific analyses, which allows us to evaluate model performance within clinically distinct populations that receive standardized, subtype-specific treatment. BRIGHT achieves an AUC of 0.766 (95%CI: 0.638-0.881) for TNBC, 0.765 (95%CI: 0.709-0.815) for HR-positive on the internal validation set, 0.642 (95%CI: 0.534-0.748) for TNBC, 0.666 (95%CI: 0.632-0.698) for HR-positive on the external validation cohort. In addition, we specifically evaluate BRIGHT on the challenging task of predicting response to neoadjuvant immunotherapy. Despite being trained on an extremely limited cohort of only 180 samples, BRIGHT demonstrated relatively more stable predictive performance compared to benchmark PFMs (Figure 4d), achieving an average AUC of 0.695. Interpretability analysis further revealed that BRIGHT's predictions are grounded in the histomorphology of tumor immune microenvironment (TIME). For the immune checkpoint blockade (ICB) responder, BRIGHT identifies immune-hot phenotype with highlighted rich TILs. While for the ICB non-responder, BRIGHT captures immune-cold phenotype with sparse TILs (Figure 4e). This finding aligns closely with established clinical evidence indicating that patients exhibiting a more active TIL-rich tumor-immune microenvironment are more likely to benefit from immunotherapy<sup>39</sup>. The model's ability to visually localize the TIME features directly from H&E slides provides a cost-effective and trustworthiness solution for patient stratification, potentially guiding treatment selection in clinical practice. Comprehensive performance metrics for each model and therapeutic response prediction tasks are provided in Supplementary Table S11-S12.

### **BRIGHT can stratified patient survival outcome**

Predicting long-term clinical outcomes, such as overall survival (OS) and disease-free survival (DFS), from histopathology images remains a challenging yet clinically important task in breast oncology. Here, we investigate whether BRIGHT can extract prognostically informative features from routine diagnostic H&E slides and thereby improve risk stratification beyond standard clinicopathological variables.

We first evaluate the prognostic performance of BRIGHT on the entire TCGA-BRCA cohort for both OS and DFS. Under a 10-fold cross-validation setting, BRIGHT consistently outperforms all PFMs, achieving a concordance index (C-index) of 0.711 for OS and 0.768 for DFS (Figure 5a). Patients are subsequently stratified into high-risk and low-risk groups using the median risk score derived from the training set. Patients classified as high risk exhibit significantly worse survival outcomes compared with those in the low-risk group (Figure 5b). Together, these results demonstrate that BRIGHT effectively captures survival-associated information from H&E slides and enables robust prognostic stratification in breast cancer. We next assess BRIGHT's prognostic performance in the TNBC cohort from C1.TMUCIH. Consistent with the findings in the overall cohort, BRIGHT achieves strong risk stratification in the TNBC cohort, yielding a C-index of 0.787 for OS in the validation set. Furthermore, in multivariable Cox regression analyses incorporating the BRIGHT-defined risk group (high-risk vs low-risk) and established clinical covariates (e.g., age, pTNM stage, and tumor laterality), BRIGHT-based risk stratification remains an independent predictor of survival outcomes. In the TCGA-BRCA cohort, the BRIGHT-defined risk group is independently associated with both OS (hazard ratio [HR]: 2.71; 95% confidence interval [CI]: 1.71–4.28;  $P < 0.05$ ) and DFS (HR: 3.08; 95%

CI: 1.27–7.48;  $P < 0.05$ ). Similarly, in the TNBC subgroup, BRIGHT maintains strong prognostic significance for OS (HR: 4.10; 95% CI: 1.94–8.69;  $P < 0.05$ ) (Figure 5c). Comprehensive performance metrics for each model and survival analysis tasks are provided in Supplementary Table S13-S16.

## Discussion

In this study, we introduce BRIGHT, the first collaborative generalist-specialist pathology foundation model (PFM) specifically designed for breast oncology. Our work addresses a critical gap in computational pathology that lack of organ-specific PFM capable of handling the full clinical spectrum within a specialized domain. By curating the largest multi-institutional benchmarking cohorts for breast pathology to date and employing a novel dual-pathway architecture, we demonstrated that BRIGHT not only sets a new state-of-the-art, outperforming leading generalist PFMs (UNlv2<sup>21</sup>, Virchow2<sup>22</sup> and CONCHv1.5<sup>17</sup>), across a comprehensive spectrum of 24 internal and 10 external clinical tasks but also establishes the collaborative generalist-specialist paradigm as a feasible solution for developing high-fidelity organ-specific AI. This paradigm moves the CPath field a step forward that transforming the generalist PFM into a specialist domain and achieving comprehensive, high-level performance within a single, complex organ system.

BRIGHT's superior performance across diagnostic, predictive, and prognostic tasks underscores the intrinsic value of integrating domain-specific knowledge. In core diagnostic tasks from cancer detection to complex multi-class subtyping, BRIGHT achieved exceptional accuracy on a natural-distribution validation cohort, highlighting its potential for reliable clinical decision support and workload reduction. More significantly, its ability to predict key molecular biomarkers (including the challenging three-tier HER2 classification and PD-L1 status) directly from H&E slides with high performance demonstrates a transformative potential for pre-screening and streamlining the diagnostic workflow. The estimated reduction in IHC testing presents a tangible path toward cost-effective and rapid precision oncology.

In predicting response to neoadjuvant therapy, BRIGHT provides accurate and subtype-stratified predictions. Its capacity to identify “immune-hot” versus “immune-cold” tumor immune microenvironments from routine H&E slides offers a potentially practical, cost-effective tool for immunotherapy patient selection, aligning with established biological principles<sup>39</sup>. Furthermore, BRIGHT's derived risk scores offered independent prognostic value for survival outcomes, complementing and enhancing traditional clinicopathological variables, which may contribute to more personalized treatment strategies.

The collaborative architecture of BRIGHT directly tackles the limitations of current generalist PFMs by harmonizing breadth with depth. While multi-organ pretraining provides a robust foundation of generalist histomorphological patterns, it may dilute subtle, organ-specific diagnostic features critical for specialist interpretation. BRIGHT resolves this by maintaining a frozen, well-pretrained generalist encoder (Virchow2<sup>22,30</sup>) to preserve broad knowledge, while a parallel and efficiently fine-tuned specialist pathway (via LoRA<sup>31</sup>) deepens expertise in breast-specific pathology. This design enables complementary feature integration, where the generalist pathway captures universal representations while the specialist pathway refines domain-specific discriminative patterns, thereby enhancing overall representational capacity. Moreover, this approach is highly parameter- and data-efficient, as it leverages well-trained PFM from millions of WSIs and thus avoids the prohibitive cost of training a comparably outstanding specialist model entirely from scratch. This algorithmic design is validated not only by BRIGHT's outperformance of all benchmark generalist PFMs but also by the superior interpretability of its attention maps, which align accurately with known pathological landmarks and biomarker expression patterns. This collaboration between generalist robustness and specialist precision is a core conceptual contribution of our work.

Despite its strengths, our study has several limitations. First, while our cohorts are the largest among current PFM studies, they are still retrospective. Prospective, multi-center clinical trials are needed to definitively establish BRIGHT's impact on diagnostic accuracy, workflow efficiency and patient outcomes. Second, the current model is designed for H&E-stained slides. Integrating multimodal data, such as immunohistochemistry, genomic profiles and pathology report<sup>40,41</sup> within the foundation model framework could enhance even more comprehensive representation and knowledge and expand the model capability to cross-modal tasks like visual question answering<sup>42</sup> and high-dimensional spatial-omics generation<sup>43,44</sup>.

In conclusion, BRIGHT demonstrates the potential value of a collaborative generalist-specialist paradigm to meet the diverse and specialized clinical demands of breast pathology. Through large-scale pre-training on breast histology and comprehensive validation across diagnostic, predictive, and prognostic tasks, the model delivers robust, expert-level performance. Our study, combining systematic multi-institutional data curation, a novel dual-pathway architecture and rigorous clinical benchmarking, provides a delightful direction for developing high-fidelity, organ-specific foundation models in oncology. These findings highlight a promising pathway for advancing next-generation PFM in other medical specialties by transitioning from generalist breadth to specialist depth. This will be essential for delivering precise and personalized care, ultimately lighting a ‘BRIGHT’ path toward improved outcomes for cancer patients.

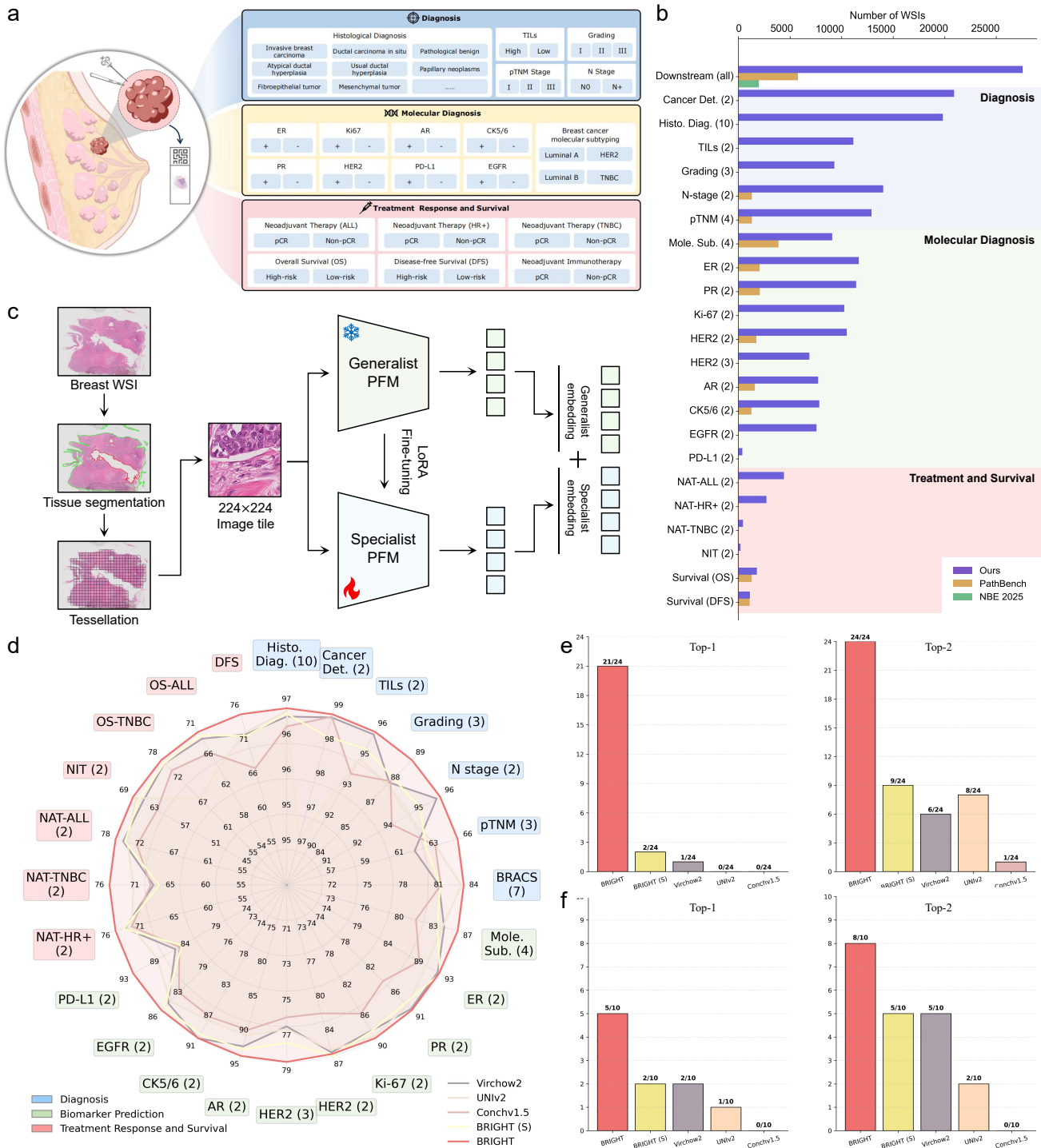


**Figure 1. Overview of BRIGHT study.** **a**, Schematic of the clinical spectrum covered by the study, encompassing diagnostic subtyping, molecular biomarker prediction, treatment response assessment, and long-term survival prediction in breast oncology. **b**, Distribution of datasets used for the development and evaluation of each downstream clinical prediction task. BRIGHT covers wider clinical tasks and more benchmarking data than existing benchmarking studies. **c**, Architecture of BRIGHT. A leading generalist pathology foundation model (PFM, Virchow2) is specialized for breast pathology via Low-Rank Adaptation (LoRA), yielding a specialist PFM (BRIGHT (S)). The final BRIGHT model is formed by the collaborative integration of feature embeddings from both generalist and specialist encoders. **d**, BRIGHT generally outperforms three leading PFMs and our specialist model BRIGHT (S) in 21 internal validation benchmarks. **e, f**, Model ranking summary. The number of tasks (among 24 internal (**e**) and 10 external (**f**) benchmarks) in which each foundation model achieved top-1 (left bars) or top-2 (right bars) performance based on AUROC for classification tasks and C-index for survival prediction tasks.

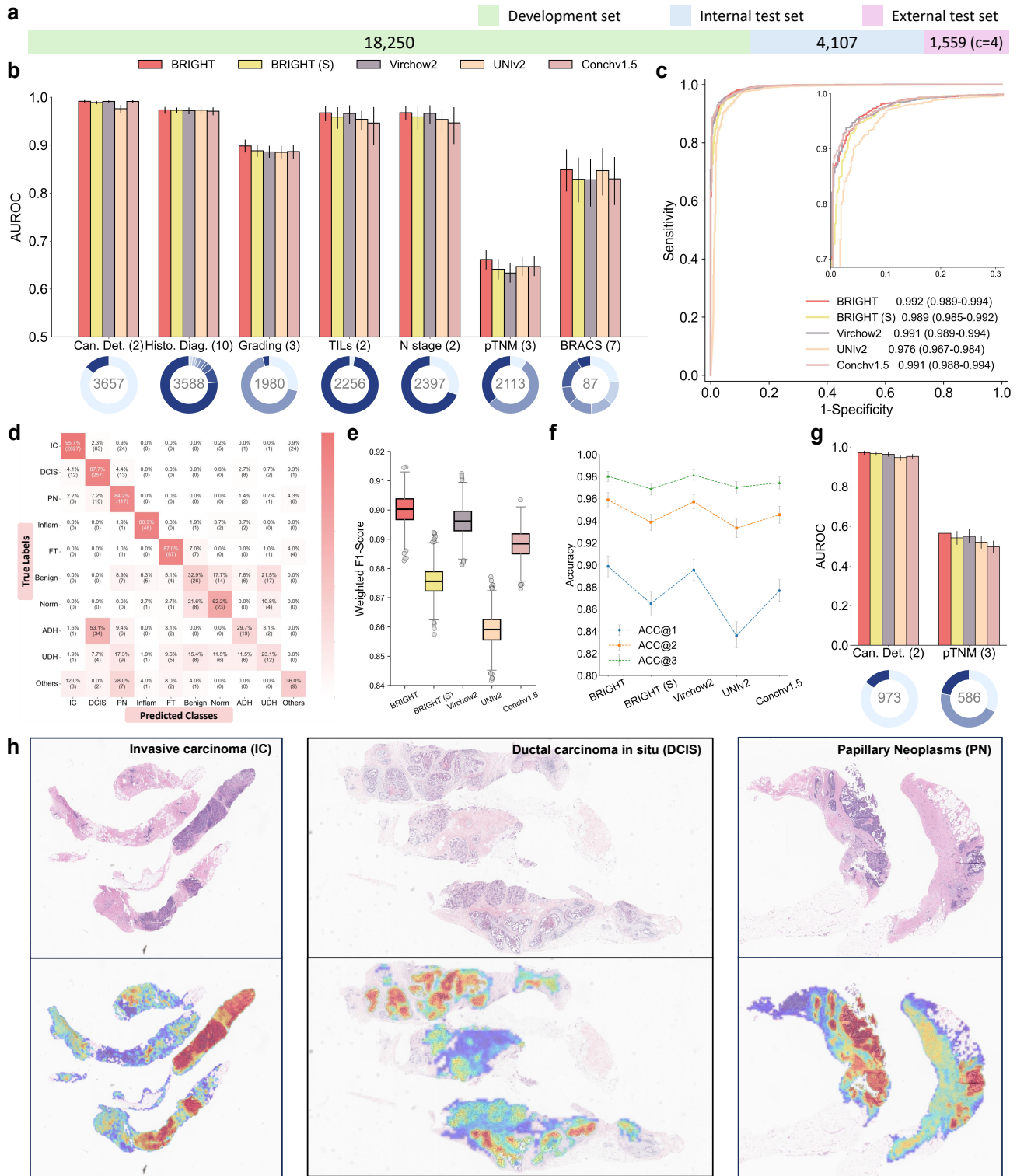


**Figure 2. Performance of PFMs on diagnostic tasks of breast pathology.** **a**, Distribution of the downstream model development, internal test and external test datasets. The number in brackets is the number of hospitals for external validation. **b**, Model performance (AUROC) across individual diagnostic tasks on the internal validation set. The pie charts below indicate the total number of WSIs and the class distribution for each task. The values in brackets indicate the numbers of categories. **c**, Receiver operating characteristic (ROC) curves for the breast cancer detection task (breast cancer vs. non-cancerous/other conditions). **d-f**, Detailed analysis of the 10-class histological diagnosis task: confusion matrix (**d**), weighted F1-scores across models (**e**), and top-n accuracy (**f**). **g**, Model performance (AUROC) on two diagnostic tasks across the combined external validation cohorts. **h**, Representative heatmap visualizations of BRIGHT on three different histological subtypes. The error bars denote the two-sided 95% confidence interval computed via 1,000 bootstrap resampling. Can. Det., Cancer detection. Histo. Diag., Histological diagnosis.

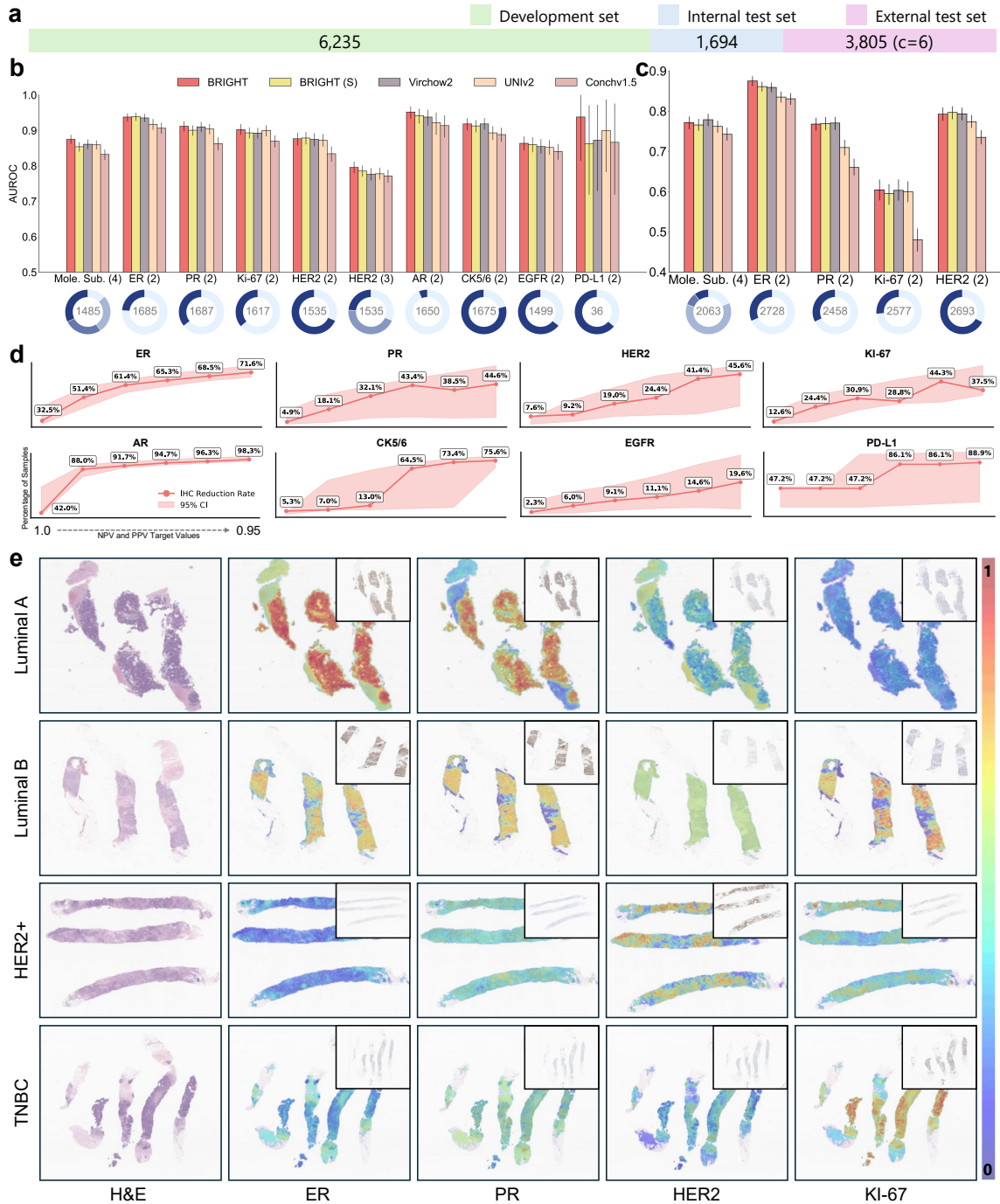


**Figure 3. Performance of PFMs on molecular subtyping and biomarker prediction tasks of breast pathology. a,** Distribution of the downstream model development, internal test and external test datasets. **b,** Model performance (AUROC) across individual tasks on the internal validation set. The values in brackets indicate the numbers of categories. **c,** Model performance (AUROC) on four biomarker prediction tasks and the molecular subtype prediction task across the combined external validation cohorts. **d,** Potential reduction in immunohistochemistry (IHC) testing, estimated by applying dual clinical thresholds, negative predictive value (NPV) and positive predictive value (PPV), to model predictions. For a given biomarker, samples with a BRIGHT-predicted probability below a predefined NPV threshold are considered true negatives, while those above a PPV threshold are considered true positives. IHC assays for these samples could be potentially waived. The proportion of such samples across the cohort yields the potential IHC assay reduction rate at those specific NPV/PPV thresholds (plotted from 1.0 to 0.95). **e,** Heatmaps generated by BRIGHT visualize the model's spatial attention when predicting key biomarkers (ER, PR, HER2, Ki-67) across the four major molecular subtypes (Luminal A, Luminal B, HER2-enriched, Triple-negative) of breast cancer. For each comparison, the corresponding diagnostic immunohistochemistry (IHC) image is shown in the top-right inset for direct visual comparison. Shaded areas and error bars denote the 95% confidence interval computed via 1,000 bootstrap resampling.

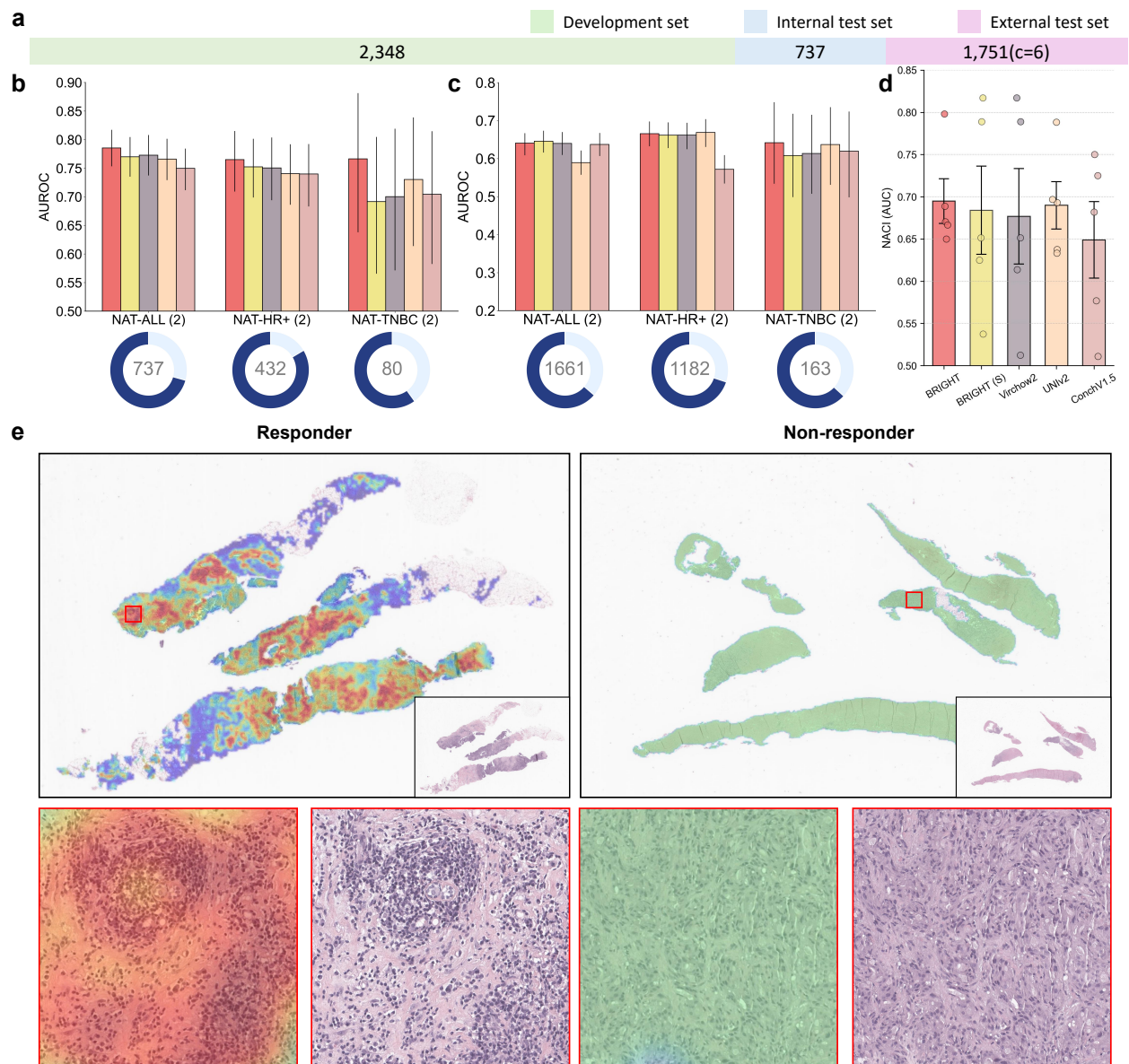


**Figure 4. Performance of PFMs in predicting breast cancer treatment response.** **a**, Distribution of the downstream model development, internal test and external test datasets. **b-c**, Model performance (AUROC) across individual neoadjuvant therapy (NAT) response prediction tasks on the internal (**b**) and external validation sets (**c**). The values in brackets indicate the numbers of categories. **d**, Performance (AUROC) of the models in predicting response to neoadjuvant immunotherapy for triple-negative breast cancer (TNBC) patients, evaluated using five-fold cross-validation. **e**, Heatmaps generated by BRIGT for a patient who responded to immune checkpoint blockade (ICB; left) and a non-responder (right). The model's attention is prominently localized to regions rich in tumor-infiltrating lymphocytes (TILs), aligning with known immunological correlates of treatment response. Error bars denote the 95% confidence interval computed via 1,000 bootstrap resampling.

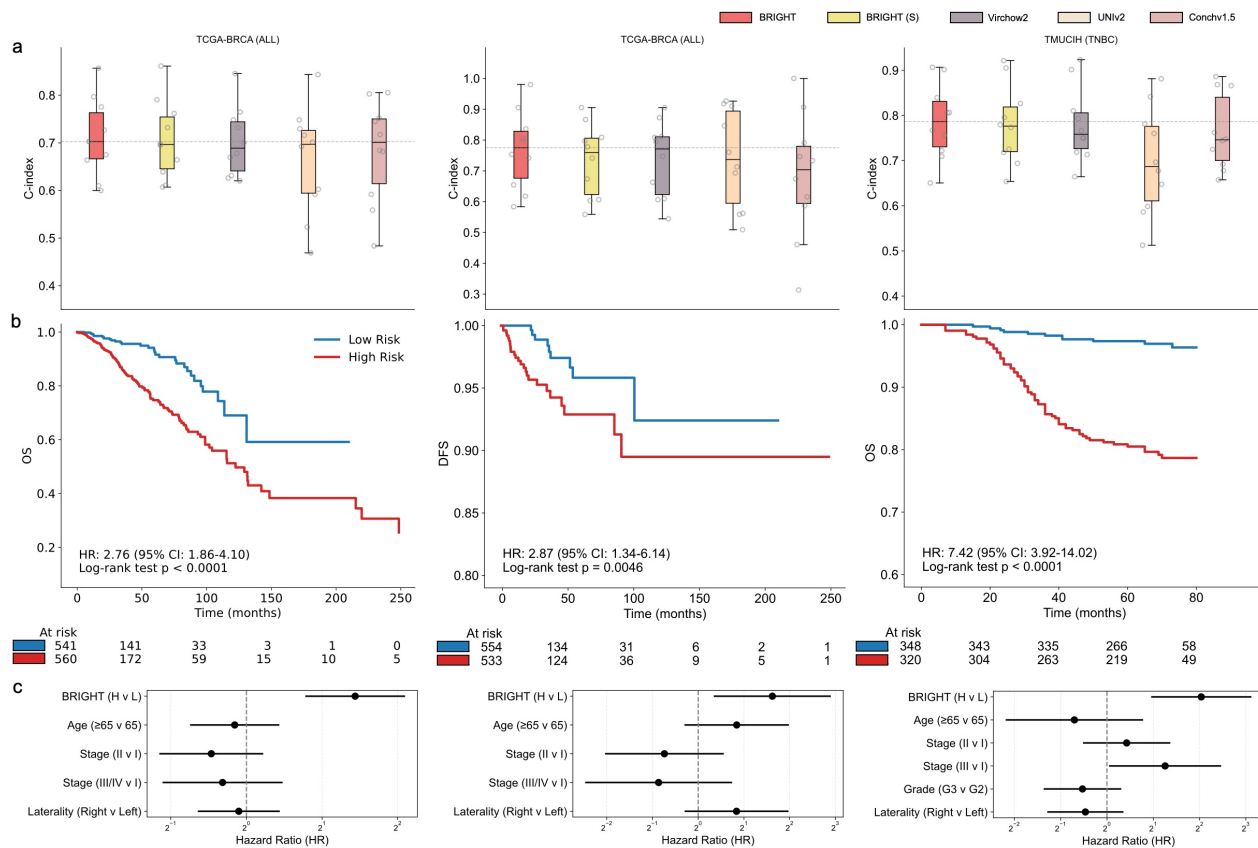


**Figure 5. Performance of PFMs in prognostic prediction.** **a**, Box plots comparing the C-index of BRIGHT with PFMs across three experimental settings: C26.TCGA-BRCA overall survival (OS), C26.TCGA-BRCA disease-free survival (DFS), and OS in the TNBC cohort of the C1.TMUCIH. Each box summarizes the C-index values obtained from all validation folds in 10-fold cross-validation. **b**, Kaplan-Meier survival curves for OS and DFS based on BRIGHT-derived risk stratification in the validation sets. Patients were stratified into high-risk (H, red) and low-risk (L, blue) groups according to the median risk score calculated from the training set. Statistical significance was assessed using a two-sided log-rank test. **c**, Forest plots of multivariable Cox proportional hazards regression analyses for OS or DFS, showing that BRIGHT risk group (H v L) is a statistically significant predictor.

## Methods

### Million-scale training dataset for BRIGHT pre-training

All data were de-identified prior to computational analysis and model development. This retrospective study did not involve direct patient recruitment or prospective intervention and was approved by the Institutional Review Boards of all participating centers. Informed consent was waived in accordance with institutional policies for research using de-identified archival specimens. To train the breast-specific pathology foundation model (BRIGHT), we construct a large-scale cohort of breast pathology whole slide images (WSIs) in this study. The foundation model training dataset comprises over 210 million non-overlapping breast pathology tiles extracted from 51,836 H&E stained WSIs from 40,203 patients, sourced from 19 independent clinical centers. The details of data collection of multiple centers are given in Supplementary Table S5. It is predominantly composed of invasive breast carcinomas, supplemented by a wide spectrum of breast lesions (e.g., fibroadenoma, usual ductal hyperplasia). All slides were digitized at  $\times 20$  (0.5 mpp) or  $\times 40$  (0.25 mpp) magnification.

### BRIGHT architecture and training

BRIGHT is built upon a dual-pathway architecture consisting of a generalist encoder and a specialist encoder with identical network structure, Vision Transformer 'huge' architecture (ViT-H/14)<sup>45</sup>. For the generalist encoder, we apply an open-source PFM (Virchow2<sup>22,30</sup>) trained on the largest dataset to date with over 3 million pan-cancer WSIs. To adapt this generalist representation to the domain of breast pathology, we employ the widely used DINOv2<sup>12</sup> as the self-supervised learning strategy and adapt low-rank adaptation (LoRA)<sup>31</sup> as a parameter-efficient fine-tuning strategy, yielding the specialist encoder BRIGHT

(S). Specifically, all parameters of the Virchow2 backbone remain frozen, and lightweight LoRA modules are injected into the query, key and value projection matrices of each self-attention layer. These LoRA modules employ a low-rank decomposition with rank 8, enabling efficient domain adaptation by updating only a small number of additional parameters. This design substantially reduces training and storage costs while maintaining the representational capacity of original model. The number of trainable parameters after LoRA injection is 24.45M with total parameters 655.60M. BRIGHT was trained using 16 NVIDIA A800 GPUs.

### **BRIGHT embedding**

For an input histopathology tile of size  $224 \times 224$  pixels, the final BRIGHT embedding was constructed by concatenating the 2560-dimensional feature vector from the specialist encoder BRIGHT (S) with the 2560-dimensional feature vector from the generalist Virchow2 encoder, resulting in a 5120-dimensional representation. The BRIGHT embedding explicitly integrates complementary features with both breast-specific patterns and pan-cancer histomorphological primitives, providing a richer and more discriminative representation for downstream tasks.

### **Aggregator for downstream tasks**

For the downstream task training and evaluation, we apply a widely used multiple-instance learning (MIL) aggregator (CLAM)<sup>32</sup> to integrate tile-level features into a slide-level prediction. The aggregator receives the set of tile embeddings from a WSI as input and outputs a task-specific prediction. For each downstream task, the BRIGHT encoders were frozen, and only the aggregator network was trained from scratch using labeled data from the respective benchmarking dataset.

### **Benchmarking datasets**

To comprehensively evaluate the performance of BRIGHT across the full clinical spectrum of breast pathology, we constructed the largest multi-institutional benchmarking dataset to date, including 24 private cohorts and two public datasets (TCGA-BRCA<sup>46</sup> and BRACS<sup>33</sup>). This resource integrates a diverse collection of public and private data, encompassing diagnostic, prognostic, and predictive tasks. A detailed breakdown of sample sizes, slide counts, and associated clinical endpoints for each dataset is provided in Supplementary Table S1-S2.

The primary cohort for downstream task development was derived from Tianjin Medical University Cancer Institute and Hospital (C1.TMUCIH). To reflect real-world clinical prevalence, data were consecutively collected without selection based on diagnosis, with exclusions applied only for insufficient image quality or incomplete clinical annotation. To ensure a robust and representative internal evaluation, a held-out validation cohort was constructed, comprising all consecutive patients undergoing breast biopsy during the full calendar year of 2024 at C1.TMUCIH. This temporal hold-out strategy preserves the natural, unselected case distribution encountered in routine practice.

For each downstream task within the internal cohort, the corresponding dataset was randomly split at the patient level into an 80% training set for model development and a 20% validation set for hyperparameter tuning and model selection. For patients with multiple slides, all slides from the same patient were assigned to the same split to prevent data leakage. Critically, all WSIs in both internal validation and external validation datasets used for downstream task evaluation are strictly held out from the BRIGHT foundation model's pre-training phase, ensuring an unbiased assessment of its generalizable feature representations.

### **Label extraction**

Clinical and pathological labels for diagnostic and biomarker prediction tasks, including breast cancer detection, histopathological diagnosis, Nottingham grade, tumor-infiltrating lymphocyte (TIL) density, pTNM stage, biomarker status (ER, PR, HER2, etc.), and molecular subtype, were extracted directly from standardized pathology reports. Treatment response labels for neoadjuvant therapy (NAT) and neoadjuvant immunotherapy (NIT) were defined based on postoperative pathological assessment of pathological complete response (pCR vs. non-pCR). Long-term survival endpoints, including overall survival (OS) and disease-free survival (DFS), were obtained from maintained clinical follow-up records. Detailed definitions for each label, including specific diagnostic criteria, biomarker thresholds, and outcome measures, are provided in Supplementary Table S4.

### **Statistical analysis**

Model performance for diagnostic, biomarker prediction, and treatment response tasks was evaluated using the area under the receiver operating characteristic curve (AUROC). Survival prediction performance was assessed with the concordance index (C-index). All performance metrics were reported based on 10-fold cross-validation. For survival analyses, patients were stratified into low- and high-risk groups based on the median risk score derived from the training set. Survival probabilities were estimated using the Kaplan-Meier method, and differences between risk groups were compared with the log-rank test. Hazard ratios (HRs) and corresponding 95% CIs were calculated using multivariable Cox proportional hazards models, as indicated in the respective results sections.

## Authors' Disclosures

The authors declare no competing interests.

## Authors' contributions

X.G. and Z.L. contributed to study conception and coordination, building a cross-center partnership and research team and getting data sharing agreements. C.H. and J.L. developed infrastructure and trained models throughout the study worked on drafting and revising the manuscript. J.Z., M.Z., F.M., N.M. and F.L. revised the manuscript. Y.J. and J.H. performed evaluation and analysis. Z.X. and W.L. contributed as research advisors. L.W., J.C., Q.L., W.W., L.C., W.Y., Z.C., X.W., J.Y., X.J., B.L., H.S., J.L., C.L., Y.C., Y.D., X.Q., L.Y., Y.Y., G.G., Y.L., Y.Y., L.Z., C.L., T.Z., Z.S., C.L., X.Z. and J.X. worked on data preparation.

## Acknowledgements

This work was funded Noncommunicable Chronic Diseases-National Science and Technology Major Project (2024ZD0531100, 2024ZD0531101); Key Program of the National Natural Science Foundation of China (82530070); Tianjin Key Medical Discipline Construction Project (TJYXZDXK-3-016C); Tianjin Medical University Cancer Institute & Hospital Medical Technology Innovation Capability Support and Enhancement Project (CXZC-YS202502); National Natural Science Foundation of China (82572321 and 82372044); Natural Science Foundation for Distinguished Young Scholars of Guangdong Province (2023B1515020043); China Postdoctoral Science Foundation (2025M772908); National Science Foundation for Young Scientists of China (82502464 and 82402228).

## Data availability

Publicly available data used in this study include the TCGA-BRCA dataset, accessible via the NIH Genomic Data Commons (<https://portal.gdc.cancer.gov>), and the BRACS dataset, accessible via the official repository (<https://www.bracs.icar.cnr.it/>). All in-house patient data were retrospectively collected, fully de-identified, and utilized under institutional review board approvals. Due to patient privacy and institutional data governance policies, these private datasets are not publicly available. Researchers interested in accessing specific subsets of the in-house data for academic, non-commercial purposes may submit a formal data use proposal to the corresponding author. Such requests will be reviewed on a case-by-case basis to ensure compliance with ethical, privacy and regulatory obligations.

## Code availability

The source code and the BRIGHT model will be released upon acceptance.

## References

1. Marra, A. *et al.* Artificial intelligence entering the pathology arena in oncology: current applications and future perspectives. *Annals Oncol.* (2025).
2. LeCun, Y., Bengio, Y. & Hinton, G. Deep learning. *nature* **521**, 436–444 (2015).
3. Lu, M. Y. *et al.* Ai-based pathology predicts origins for cancers of unknown primary. *Nature* **594**, 106–110 (2021).
4. Bulten, W. *et al.* Artificial intelligence for diagnosis and gleason grading of prostate cancer: the panda challenge. *Nat. medicine* **28**, 154–163 (2022).
5. Wagner, S. J. *et al.* Transformer-based biomarker prediction from colorectal cancer histology: A large-scale multicentric study. *Cancer cell* **41**, 1650–1661 (2023).
6. Campanella, G. *et al.* Real-world deployment of a fine-tuned pathology foundation model for lung cancer biomarker detection. *Nat. Medicine* **31**, 3002–3010 (2025).
7. Gustav, M. *et al.* Assessing genotype- phenotype correlations in colorectal cancer with deep learning: a multicentre cohort study. *The Lancet Digit. Heal.* **7** (2025).
8. Ogier du Terrail, J. *et al.* Federated learning for predicting histological response to neoadjuvant chemotherapy in triple-negative breast cancer. *Nat. medicine* **29**, 135–146 (2023).
9. Yuan, W. *et al.* Pancancer outcome prediction via a unified weakly supervised deep learning model. *Signal transduction targeted therapy* **10**, 285 (2025).
10. Skrede, O.-J. *et al.* Deep learning for prediction of colorectal cancer outcome: a discovery and validation study. *The Lancet* **395**, 350–360 (2020).
11. Amgad, M. *et al.* A population-level digital histologic biomarker for enhanced prognosis of invasive breast cancer. *Nat. medicine* **30**, 85–97 (2024).
12. Oquab, M. *et al.* Dinov2: Learning robust visual features without supervision. *arXiv preprint arXiv:2304.07193* (2023).
13. Radford, A. *et al.* Learning transferable visual models from natural language supervision. In *International conference on machine learning*, 8748–8763 (PmLR, 2021).
14. Moor, M. *et al.* Foundation models for generalist medical artificial intelligence. *Nature* **616**, 259–265 (2023).
15. Huang, Z., Bianchi, F., Yuksekgonul, M., Montine, T. J. & Zou, J. A visual–language foundation model for pathology image analysis using medical twitter. *Nat. medicine* **29**, 2307–2316 (2023).
16. Wang, X. *et al.* A pathology foundation model for cancer diagnosis and prognosis prediction. *Nature* **634**, 970–978 (2024).
17. Lu, M. Y. *et al.* A visual-language foundation model for computational pathology. *Nat. medicine* **30**, 863–874 (2024).
18. Xiang, J. *et al.* A vision–language foundation model for precision oncology. *Nature* **638**, 769–778 (2025).
19. Lu, M. Y. *et al.* A multimodal generative ai copilot for human pathology. *Nature* **634**, 466–473 (2024).
20. Xu, H. *et al.* A whole-slide foundation model for digital pathology from real-world data. *Nature* **630**, 181–188 (2024).
21. Chen, R. J. *et al.* Towards a general-purpose foundation model for computational pathology. *Nat. medicine* **30**, 850–862 (2024).
22. Vorontsov, E. *et al.* A foundation model for clinical-grade computational pathology and rare cancers detection. *Nat. medicine* **30**, 2924–2935 (2024).
23. Yang, Z. *et al.* A foundation model for generalizable cancer diagnosis and survival prediction from histopathological images. *Nat. Commun.* **16**, 2366 (2025).
24. Ma, J. *et al.* A generalizable pathology foundation model using a unified knowledge distillation pretraining framework. *Nat. Biomed. Eng.* 1–20 (2025).
25. Xiong, C., Chen, H. & Sung, J. J. A survey of pathology foundation model: Progress and future directions. *arXiv preprint arXiv:2504.04045* (2025).
26. Mahmood, F. A benchmarking crisis in biomedical machine learning. *Nat. Medicine* **31**, 1060–1060 (2025).
27. Ma, J. *et al.* Pathbench: A comprehensive comparison benchmark for pathology foundation models towards precision oncology. *arXiv preprint arXiv:2505.20202* (2025).
28. Neidlinger, P. *et al.* Benchmarking foundation models as feature extractors for weakly supervised computational pathology. *Nat. biomedical engineering* 1–11 (2025).

29. Campanella, G. *et al.* A clinical benchmark of public self-supervised pathology foundation models. *Nat. Commun.* **16**, 3640 (2025).
30. Zimmermann, E. *et al.* Virchow2: Scaling self-supervised mixed magnification models in pathology. *arXiv preprint arXiv:2408.00738* (2024).
31. Hu, E. J. *et al.* Lora: Low-rank adaptation of large language models. *ICLR* **1**, 3 (2022).
32. Lu, M. Y. *et al.* Data-efficient and weakly supervised computational pathology on whole-slide images. *Nat. biomedical engineering* **5**, 555–570 (2021).
33. Brancati, N. *et al.* Bracs: A dataset for breast carcinoma subtyping in h&e histology images. *Database* **2022**, baac093 (2022).
34. Modi, S. *et al.* Trastuzumab deruxtecan in previously treated her2-low advanced breast cancer. *New Engl. J. Medicine* **387**, 9–20 (2022).
35. Wong, C. *et al.* Ai-driven mri biomarker for triple-class her2 expression classification in breast cancer: a large-scale multicenter study. *Breast Cancer Res.* **27**, 166 (2025).
36. Cortes, J. *et al.* Pembrolizumab plus chemotherapy in advanced triple-negative breast cancer. *New Engl. J. Medicine* **387**, 217–226 (2022).
37. Loibl, S. *et al.* Early breast cancer: Esmo clinical practice guideline for diagnosis, treatment and follow-up. *Annals Oncol.* **35**, 159–182 (2024).
38. Schmid, P. *et al.* Event-free survival with pembrolizumab in early triple-negative breast cancer. *New Engl. J. Medicine* **386**, 556–567 (2022).
39. El Bairi, K. *et al.* The tale of tils in breast cancer: a report from the international immuno-oncology biomarker working group. *NPJ breast cancer* **7**, 150 (2021).
40. Xu, Y. *et al.* A multimodal knowledge-enhanced whole-slide pathology foundation model. *Nat. Commun.* (2025).
41. Yan, S. *et al.* A multimodal vision foundation model for clinical dermatology. *Nat. Medicine* 1–12 (2025).
42. He, X., Zhang, Y., Mou, L., Xing, E. & Xie, P. Pathvqa: 30000+ questions for medical visual question answering. *arXiv preprint arXiv:2003.10286* (2020).
43. Li, Z. *et al.* Ai-enabled virtual spatial proteomics from histopathology for interpretable biomarker discovery in lung cancer. *Nat. Medicine* 1–14 (2026).
44. Valanarasu, J. M. J. *et al.* Multimodal ai generates virtual population for tumor microenvironment modeling. *Cell* (2025).
45. Dosovitskiy, A. An image is worth 16x16 words: Transformers for image recognition at scale. *arXiv preprint arXiv:2010.11929* (2020).
46. Weinstein, J. N. *et al.* The cancer genome atlas pan-cancer analysis project. *Nat. genetics* **45**, 1113–1120 (2013).